Published in final edited form as:
Sci Transl Med. 2012 August 29; 4(149): 149ra119. doi:10.1126/scitranslmed.3003594.

A Dense Poly(ethylene glycol) Coating Improves Penetration of Large Polymeric Nanoparticles within Brain Tissue

Elizabeth A. Nance[1,2,†], **Graeme F. Woodworth**[1,3,†], **Kurt A. Sailor**[4], **Ting-Yu Shih**[2], **Qingguo Xu**[1,6], **Ganesh Swaminathan**[2], **Dennis Xiang**[2], **Charles Eberhart**[1,5,6], and **Justin Hanes**[1,2,3,6,*]

[1]Center for Nanomedicine at the Wilmer Eye Institute, Johns Hopkins University School of Medicine, Baltimore, MD 21231, USA

[2]Department of Chemical and Biomolecular Engineering, Johns Hopkins University, Baltimore, MD 21218 (USA)

[3]Department of Neurosurgery, Johns Hopkins University School of Medicine, Baltimore, MD 21205 (USA)

[4]Department of Neuroscience, Institute for Cellular Engineering, Johns Hopkins University School of Medicine, Baltimore, MD 21205 (USA)

[5]Department of Pathology, The Wilmer Eye Institute, Johns Hopkins University School of Medicine, Baltimore, MD 21231 (USA)

[6]Department of Ophthalmology, The Wilmer Eye Institute, Johns Hopkins University School of Medicine, Baltimore, MD 21231 (USA)

Abstract

Prevailing opinion suggests that only substances up to 64 nm in diameter can move at appreciable rates through the brain extracellular space (ECS). This size range is large enough to allow diffusion of signaling molecules, nutrients, and metabolic waste products, but too small to allow efficient penetration of most particulate drug delivery systems and viruses carrying therapeutic genes, thereby limiting effectiveness of many potential therapies. We analyzed the movements of nanoparticles of various diameters and surface coatings within fresh human and rat brain tissue *ex vivo* and mouse brain *in vivo*. Nanoparticles as large as 114-nm in diameter diffused within the human and rat brain, but only if they were densely coated with poly(ethylene glycol) (PEG). Using these minimally adhesive PEG-coated particles, we estimated that human brain tissue ECS has some pores larger than 200 nm, and that more than one-quarter of all pores are ≥100 nm. These findings were confirmed *in vivo* in mice, where 40- and 100-nm, but not 200-nm, nanoparticles,

*Corresponding author: hanes@jhu.edu.
†Authors contributed equally to this work

Supplementary materials
Methods (49–51)
Movie S1. Multiple particle tracking of 91-nm PLGA NPs in normal rat brain tissue ex vivo.
Movie S2. Multiple particle tracking of 83-nm paclitaxel-loaded PEG-PLGA NPs in normal rat brain tissue ex vivo.

Author contributions: G.F.W., E.A.N., and J.H. developed the concept. E.A.N. and G.F.W. designed and performed *ex vivo* experiments. G.F.W. established arrangements for human tissue. G.F.W., E.A.N., and K.A.S. designed and performed *in vivo* experiments. E.A.N. and T.-Y.S. designed and performed biodegradable particle experiments. Q.X. performed NMR experiments and analysis. E.A.N., G.F.W., T.-Y.S., G.S., and D.X. analyzed data. C.E. provided histological analysis for all tissues. E.A.N., G.F.W., and J.H. wrote the paper.

Competing interests: The content is solely the responsibility of the authors and does not necessarily represent the official views of the National Institutes of Health. E.A.N., G.F.W, and J.H. are inventors on a pending patent (International Application No.: PCT/US2011/051195) related to this work.

spread rapidly within brain tissue, only if densely coated with PEG. Similar results were observed in rat brain tissue with paclitaxel-loaded biodegradable nanoparticles of similar size (85 nm) and surface properties. The ability to achieve brain penetration with larger nanoparticles is expected to allow more uniform, longer-lasting, and effective delivery of drugs within the brain, and may find use in the treatment of brain tumors, stroke, neuroinflammation, and other brain diseases where the blood-brain barrier is compromised or where local delivery strategies are feasible.

Introduction

The blood-brain barrier (BBB) has long been considered an impediment for effective treatment and imaging of a broad range of central nervous system (CNS) diseases (1). As a result, localized strategies for delivering substances within the brain have become important (2). For example, Gliadel, a biodegradable polymer wafer loaded with carmustine that is implanted in the brain after tumor resection, was approved by the FDA in 1996 for treatment of patients with recurrent glioblastomas (GBM). This therapy improves survival of patients with GBM and HGG, and demonstrates the importance of locally administered, controlled-release polymer systems in treating brain tumors.

The BBB is also known to be disrupted by the presence of brain tumors and in other clinical situations, including during neuroinflammation, abnormal development, infection, and cerebrovascular disease (stroke, hypertension, and ischemia) (1, 3). BBB breakdown in these cases allows drugs and drug-loaded nanoparticles (NPs) up to a few hundred nanometers in diameter to bypass the endothelium that comprises the BBB and enter the brain; for example by the enhanced permeation and retention (EPR) effect (4) in tumors and at sites of inflammation. Systemic drug delivery to the CNS by NPs in these cases has been shown to have positive therapeutic effects in various animal disease models, including brain tumors (5), neuroinflammation (6), and ischemia (7). In addition, it has been shown that NPs coated with poly(ethylene glycol) (PEG) accumulate more efficiently in the brain with a compromised BBB compared to similar uncoated NPs (8, 9), at least partly as a result of the greatly improved blood circulation time and the “stealth” nature of PEG-coated particles (10).

Methods that improve drug penetration within the brain parenchyma (11) have also been shown to enhance therapeutic efficacy in animal models. For example, localized convection-enhanced delivery (CED) has been used to widely distribute drugs (12), macromolecules (13), and nanocarriers (14) in the brain, leading to enhanced efficacy compared to systemic therapy. In addition, Jain and coworkers have shown that the EPR effect is heterogeneous in tumors, and that increased interstitial pressure in tumors can limit drug penetration (15), thereby motivating the need for NPs that can penetrate parenchyma once within the brain. However, it has been suggested that NPs must be very small (<64 nm) in order to penetrate within the brain parenchyma through the extracellular space (ECS) (16). Openings below this size are large enough to allow diffusion of proteins and small molecules, while being small enough to limit the movement of many nanoparticulate drug delivery or imaging systems. Thus, despite the need to deliver drugs directly to brain tissue, the human brain ECS is thought to pose a formidable barrier to NP penetration.

We therefore sought to determine whether dense coatings with low molecular weight PEG might allow larger NPs (up to 200 nm) to penetrate the brain parenchyma. The ability to achieve brain penetration with larger NPs will enable higher drug-loading efficiency and payload, greater dispersion of drugs, and longer drug release—factors that enhance translational potential of any nanotherapeutic approach because of the known correlation with efficacy (17). We used rodent brain tissue *in vivo* and *ex vivo*, and fresh human tissue

ex vivo, to study brain ECS pore size and NP diffusion within the brain. Real-time multiple particle tracking (MPT) indicated that NPs at least 114 nm in diameter were capable of penetrating human and rat brain tissue. In support of these findings, the movements of the same NPs in the living mouse brain were directly visualized and compared using *in vivo* particle tracking through a cranial window. A paclitaxel-loaded NP system with similar size and surface characteristics as the conventional PEG-coated particles showed that therapeutic delivery for CNS disorders is possible.

Results

Particle tracking in human brain tissue *ex vivo*

Having previously shown that transport of unexpectedly large NPs through mucus gels depends on their surface coatings (18, 19), we hypothesized here that similar modifications of particle physicochemical properties could provide a more accurate estimate of the pore size range within the human brain ECS. Fluorescent polystyrene (PS) particles with dense PEG or carboxyl (COOH) coatings (Table 1) were added to freshly dissected human brain cortex tissue and the particle Brownian motions were quantified using *ex vivo* high-resolution MPT (Supplementary Methods). The PEG-coated particles used were 10–20 nm larger than the COOH-coated particles and had a near-neutral net surface charge (Table 1). PEG-coated PS particles have surfaces dominated by PEG, which prevents aggregation in artificial cerebrospinal fluid (ACSF), as indicated by the low polydispersity index (PDI) values provided in Table 1. The 40- and 100-nm PEG-coated particles rapidly penetrated human brain tissue, as exhibited by ensemble geometric mean square displacements (MSD) that were 2300- and 1500-fold higher than similarly sized COOH-coated particles (Fig. 1A; Table 1). PEG-coated 40-and 100-nm particles diffused only 37 and 36 times slower, respectively, in the human brain tissue *ex vivo* than in ACSF, whereas standard COOH-coated PS particles of similar sizes moved 54,000–86,000 times slower in brain than in ACSF (Table 1). Therefore, dense PEG coatings allowed 40-nm and 100-nm particles to experience the brain ECS as a permeable viscoelastic liquid rather than an impermeable viscoelastic solid, as seen previously with PEGylated NPs with diameters smaller than the average mesh size in human mucus samples (18). The similar, rapid transport rates of 40- and 100-nm PEG-coated particles in the human brain tissue is expected only if the ECS pore size cut-off is greater than 100 nm.

In contrast, 200-nm PEG-coated particles diffused 1600-times slower in the human brain tissue *ex vivo* than in ACSF, or approximately 45-fold slower than the 100-nm PEG-coated particles in the brain (Fig. 1A). The expected difference for diffusion rates of 100- and 200-nm particles—defined by a ratio of the theoretical diffusion coefficient D_2/D_1 (where D is defined by the Stokes-Einstein equation)—would be only 2-fold for non-adhesive NPs, unless there was a ECS pore-size cut-off between 100 and 200 nm. The density and viscosity of ACSF are the same as water at physiological pH; therefore, ACSF and water are assumed to be equal for this study. Representative particle trajectories for both PEG-coated and COOH-coated particles at all sizes studied in human brain tissue are provided in Figure 1B. COOH-coated particles exhibited highly constrained motion regardless of size, presumably owing to adhesive interactions, whereas the same particles densely coated with PEG exhibited diffusive motion for 40- and 100-nm particles, but hindered motion for 200 nm. For all NP sizes studied, 100% of COOH-coated particles were immobilized (MSDs below the resolution of the microscope) or strongly hindered (MSDs smaller than the particle diameter) within the ECS. These observations suggest that, regardless of PS particle size, electrostatic (negatively charged carboxylate surface) and/or hydrophobic (exposed PS surfaces) interactions limit uncoated NP diffusion within the brain.

To estimate the effective pore size range in the human brain ECS, the Amsden obstruction scaling model (20) for entangled and cross-linked gels was fit to the MSD data in Figure 1A, as shown previously for estimating the pore size in human mucus (18, 21). Human brain tissue ECS was found to have pores as large as 225 nm, with approximately 28% of the pores larger than 100 nm (Fig. 1C). The smallest pores experienced by the probe particles were less than 40 nm, which is similar to previous reports based on Fick's Law-derived diffusion analysis of NPs with lower-density PEG coatings (16, 22, 23).

Ex vivo tissue maintains integrity during particle tracking

The *ex vivo* brain slice model has been used extensively to study the diffusion of various substances (24), neural electrophysiology (25), and cell migration (26, 27). Histological analysis has consistently confirmed intact cytoarchitecture and functioning tissue physiology (28, 29). Representative hematoxylin and eosin (H&E)-stained sections ($n = 4$ sections for each of 5 patients at both t = 0 hours and t = 3 hours) of the initial and post-acquisition human brain tissue were examined by a pathologist (C.E.). In particular, the presence of cellular swelling, pyknotic nuclei, and ischemia were examined. No differences were observed in the brain tissue between immediate tissue removal (30 minutes) and 3 hours after tissue removal (Fig. 1D), suggesting minimal damage was introduced by tissue removal, collection, and processing. All particle-tracking experiments were conducted within this time frame.

Particle tracking in live mouse brain

The ex vivo model is limited in that it is not subject to the dynamic environment of the living brain, including the bulk flow of cerebrospinal fluid and ECS volume fraction changes that can occur. Therefore, using live-animal imaging, we directly observed NP penetration *in vivo* in mouse brains to confirm findings obtained using *ex vivo* tissue slices. Red-fluorescent, COOH-coated NPs and green-fluorescent, PEG-coated NPs with similar diameters were co-injected into the mouse cerebral cortex at a depth of 100–200 μm below the pial surface. Real-time video microscopy showed that COOH-coated particles of all sizes were uniformly stuck in the tissue, whereas 40- and 100-nm particles with dense PEG coatings penetrated up to 200 μm into the tissue within the 60-min imaging interval (Fig. 2A). PEG-coated 200-nm particles did not penetrate the brain tissue, presumably because of steric hindrance.

To further confirm these differences between size and particle coating, we performed co-injections 100–200 μm below the pial surface of PEG-coated red and green fluorescent NPs of different sizes. Similar to results observed in the human brain tissue *ex vivo*, the 40- and 100-nm PEG-coated particles penetrated farther into the mouse brain *in vivo* than the 200-nm PEG-coated particles (Fig. 2B), confirming relatively few ECS pores greater than 200 nm. Representative single-particle trajectories from separate regions within the brain showed much farther movement for the 100-nm PEG-coated particles compared to either the PEG-coated 200-nm particles or COOH-coated 100- and 200-nm particles (Fig. 2C). We were unable to consistently resolve the individual movements of 40 nm PEG-coated particles *in vivo* owing to their exceptionally fast movement in and out of the focal plane.

Drug-loaded biodegradable nanoparticles penetrate brain tissue

Biodegradable NP systems composed of block copolymers of poly(lactic-*co*-glycolic acid) (PLGA) and PEG and loaded with paclitaxel could rapidly diffuse in normal rat brain tissue *ex vivo*, whereas PLGA NPs without PEG coatings could not (movies S1 and S2). Representative particle trajectories of paclitaxel-loaded PEG-PLGA NPs (mean ± SEM: 85 ± 4 nm; −2.7 ± 0.8 mV; 2.5 wt% paclitaxel), PEG-PLGA NPs that did not contain drug

(mean ± SEM: 78 ± 3 nm; −3.5 ± 1 mV), and uncoated PLGA particles (mean ± SEM: 81 ± 3 nm; −30.1 ± 1 mV) are provided in Figure 3A.

By examining the distribution of individual particle diffusivities, we established that biodegradable PEG-PLGA NP systems exhibit a more substantial rapidly diffusing fraction (24%) compared to PLGA NP systems (Fig. 3B). The biodegradable systems tested possessed similar size characteristics compared to the 100-nm PS particles used in our studies here in human brain tissue *ex vivo* and in living mouse brains.

High PEG surface density required for NP diffusion in brain ECS

We found that a dense PEG coating on PS NPs, quantum dots (QDs), and PLGA NPs, which results in a near-neutral NP surface charge, correlated with a greater percent diffusive fraction in rat brain tissue *ex vivo* (Fig. 4 and Table 2). NP formulations with zeta (ξ)-potentials less negative than −4 mV were consistently capable of diffusing in the rat brain (5 out of 5 NP formulations). Conversely, only 1 out of 2 NP formulations with ξ-potentials between −4 and −6 mV possessed NPs that diffused, and 0 out of 6 NP formulations with ξ-potentials more negative than −6 mV were capable of diffusion (Fig. 4). Using a nuclear magnetic resonance (NMR)-based method to quantify the PEG coating density required for NPs to diffuse in the brain, we estimate that 100-nm PS NPs must possess roughly 9 PEG molecules (MW = 5 kDa) per 100 nm^2 of particle surface in order to diffuse in the rat brain tissue slice model. NPs that diffused within the brain had PEG layers in the brush regime, with $\Gamma/SA \geq 2$, where Γ is the total surface area (SA) coverage that would be provided by the PEG molecules assuming PEG conformation on the particle surface was unconstrained (Supplementary methods). NP formulations with $\Gamma/SA \leq 1.7$ did not diffuse in the rat brain slice model.

Discussion

In this study, MPT was used to analyze the diffusion rates of densely PEG-coated versus standard COOHcoated NPs of various sizes in human and rat brain tissue *ex vivo*, as well as in the living mouse brain *in vivo*. The results from three model systems aligned closely, producing surprising results: (1) the human, rat, and mouse brain ECS have 28% of pores ≥100 nm; (2) particles larger than the previously reported ECS mesh size range (upper limit of 64 nm) (16) rapidly penetrate within the brain, but only if densely coated with PEG ($\Gamma/SA \geq 2$), which minimizes adhesive interactions; and (3) all uncoated NPs—even the 40-nm particles—were essentially immobile in human, rat, and mouse brains. Large brain-penetrating NPs that contain bioactive drugs and are composed of biocompatible molecules, such as PLGA and PEG, with a long history of safe use in humans, should facilitate translation and testing of therapeutic strategies in human clinical trials.

These findings were guided by our previous work defining the particle size and surface chemistry required for NP penetration through another biologic interface. Specifically, by using minimally adhesive NPs with dense PEG coatings, we showed previously that human mucus barriers possess pores much larger than expected (18, 19, 21). Accurately defining key particle characteristics required to achieve penetration of this barrier has proven critical to the design of efficacious drug-loaded particle systems (30, 31). The ability to achieve brain penetration with larger particles (>100 nm) will enable higher drug-loading efficiency and payload, greater dispersion of drugs, and drug release over longer periods of time (17, 32). These factors are known to correlate with the efficacy of many therapeutics (11, 17) and will likely have a substantial impact on the utility of nano-sized carriers for diagnostic and therapeutic delivery to the brain. A recent study reported the construction of 100-nm gelatin particles that degraded into 10-nm particles when exposed to proteases within sarcoma tumors, with the goal of achieving better distribution with the smaller particle (33).

Although an important goal for imaging agents, the very small particle size necessary to achieve penetration makes translation of a therapeutically effective controlled drug delivery system to humans less likely. Our results suggest that this system could be redesigned to degrade into particles as large as 114 nm, which may enhance drug and imaging agent options and improve the prospects for translation to the clinic. The demonstration here of the penetration within the brain by 85-nm PLGA-PEG NPs loaded with a chemotherapeutic (paclitaxel) bodes well for testing of this strategy in human clinical trials, either as a particle administered systemically that might reach brain tumors by the EPR effect or as a particle administered directly into the brain by CED.

NPs have been shown to accumulate in the brain parenchyma following systemic administration in various disease models that have a disrupted BBB (6, 7, 34). Studies have further shown that PEG-coated polymer NPs accumulate much more efficiently in the parenchyma than do uncoated, but otherwise similar, NPs (8, 9). In these papers, the PEG-coated particles were 135–165 nm in diameter, and possessed a surface charge between −20 and −40 mV, suggesting that they may be too large and/or coated with an insufficiently dense layer of PEG to spread within the brain parenchyma following their uptake by the EPR effect. NPs coated with special surfactants, such as Polysorbate 80 (P80) (5, 34) or Poloxomer 188 (also referred to as Pluronic F68) (5, 35), or with chitosan (36) have also been shown to target the brain following systemic injection, even with an intact BBB, by adhering to and entering endothelial cells of the BBB. The NPs coated with P80 or F68 possessed surface charges in the −20 to −40 mV range, and the chitosan-coated particles were 260 nm in diameter, thereby making it unlikely that these specific particles are capable of spreading into the brain beyond the BBB endothelium. These previous papers, combined with our current findings, suggest that densely PEG-coated NPs with sizes ≤ 114 nm and a near neutral surface charge may allow both accumulation within the brain following systemic administration and efficient spread by diffusion within the brain parenchyma in diseases with an impaired BBB.

Early measurements of the ECS pore size using electron microscopy suggested the upper pore size limit was approximately 20 nm (37). In 2006, Thorne and Nicholson analyzed the diffusion limitations of macromolecules (dextrans) and 35-nm PEG-coated NPs in the rat brain using *in vivo* epifluorescence microscopy (16). From these data, the apparent diffusion coefficients were calculated and, employing a fluid-filled pore model, they suggested that the rat cortical ECS has pores as large as 38–64 nm (16). We characterized a batch of these commercially available PEG-coated QDs (35 nm, −5.1 mV) and found that they did not diffuse rapidly within the rat brain tissue *ex vivo*. We then further coated these same particles with PEG (34 nm, −3.1 mV) and found that these could penetrate more rapidly. Thus, the precise batch of the commercially available QDs used by Thorne and Nicholson may have possessed a PEG coating that was too sparse to allow for rapid penetration in the brain parenchyma and any adhesive interactions between the QDs and the ECS would result in an underestimation of brain ECS pore size.

A net negative surface charge should reduce NP electrostatic interactions within the brain owing to repulsion from negatively charged cell surfaces and extracellular matrix components (14, 38). In this study, we show that negatively charged (COOH-coated) particles with exposed hydrophobic PS regions exhibit hindered diffusion regardless of particle size. Often underappreciated, the hydrophobic interactions between particle surfaces and ECS components can be a source of adhesion (39). Adequate surface shielding (via PEG, for example) from these interactions is apparently crucial for diffusion of large particles in the brain. The formation of PEG coatings well into the brush regime likely limits exposure of hydrophobic NP surfaces that facilitate adhesion to the brain ECS. We report diffusive NP behavior for PEG conformations on 100-nm PS particles, with $\Gamma/SA \geq 2.0$,

whereas Γ/SA ≤ 1.7 was insufficient. The impact of PEG on biodegradable polymeric NPs and liposome size and surface charge has been shown to be dependent on PEG molecular weight, particle core, and PEG weight percent (30, 40, 41). The precise PEG coating densities required should be further confirmed using additional methods, such as MALDI-TOF and atomic force microscopy, and will likely depend on the material being coated.

In this study, we established that NPs at least as large as 114 nm, but smaller than 200 nm, can penetrate brain ECS if coated with a high density of 5 kDa PEG. Large brain-penetrating NPs offer a greater degree of flexibility in designing delivery systems to produce a desired effect within the human brain. Dense PEG coatings are also known to be important for enhanced NP circulation within the blood stream and entering the brain through a disrupted BBB, and are also expected to lead to greater drug distribution when used with local strategies such as CED. Although we did not test in a disease model to confirm, demonstration of an 85-nm drug-loaded biodegradable NP that penetrates within the brain parenchyma suggests that the development of drug delivery systems with the characteristics established in this paper offer promising new directions for particle-mediated delivery of therapeutic molecules in the brain. We envision that our findings may be first translated into the clinic in the treatment of malignant brain tumors owing to the poor prognosis with this disease, where NPs may access the brain via the EPR effect and then spread locally to provide a more uniform delivery of encapsulated therapeutic agents. Alternatively, the NPs may be administered locally by CED to maximize their penetration to treat invasive tumor cells. Once safety has been established, this approach may find use in treating other CNS diseases or conditions associated with a disrupted BBB. In the future, we expect new methods that enhance the delivery of NPs into the brain through an intact BBB will be developed and shown to be safe, such as high-intensity focused ultrasound (42), thus leading to widespread clinical use of PEG-coated NPs.

Materials and Methods

Nanoparticle preparation and characterization

Forty- to 200-nm red fluorescent COOH-modified polystyrene (PS) particles (Molecular Probes) were covalently modified with methoxy (MeO)-PEG-amine (NH_2) (5 kDa MW; Creative PEG Works) by carboxyl amine reaction, following a modified protocol described previously (18, 43). These two protocols were combined and optimized here to obtain dense PEG coatings, a near-neutral ξ-potential, and low PDI, for 40–200 nm PS particles. Briefly, 100 μL of PS particle suspension was washed and resuspended to 4-fold dilution in ultrapure water. An excess of MeO-PEG-NH_2 was added to the particle suspension and mixed to dissolve the PEG. *N*-Hydroxysulfosuccinimide (Sigma) was added to a final concentration of 7 mM, and 200 mM borate buffer, pH 8.2, was added to a 4-fold dilution of the starting volume. 1-Ethyl-3-(3-dimethylaminopropyl) carbodiimide (EDC, Invitrogen) was added to a concentration of 10 mM. Particle suspensions were placed on a rotary incubator for 4 hours at 25°C and then centifuged (Amicon Ultra 0.5 mL 100k MWCO; Millipore). Particles were resuspended in ultrapure water to the initial particle volume (100 μL) and stored at 4°C until use.

The net surface charge (ξ-potential), polydispersity index (PDI), and hydrodynamic diameter were measured for COOH- and PEG-coated fluorescent NPs of all sizes. Particle characterization is described in detail in Supplementary Methods.

Human and rat neocortical slice preparation

Human tissue collection was approved by the Institutional Review Board (IRB) at Johns Hopkins University. Fresh human brain cortex was removed from 5 patients undergoing

surgery for mesial temporal lobe epilepsy. Following removal, the tissue was rapidly divided into the components needed for pathological analysis; the remaining tissue was dissected to avoid the sclerotic tissue that often accompanies the disease then placed in normal saline on ice and transported immediately to the laboratory for slice preparation. Tissue was immersed in chilled ACSF (Harvard Apparatus) supplemented with 10 mM glucose. Coronal slices (n = 6 per patient) were prepared using a rodent brain slice matrix kit (Zivic Instruments). The matrix and razor blades were washed with 0.9% normal saline and placed on ice prior to inserting the excised human brain sample. Sectioning of the brain was carried out based on instrument instructions such that 1-mm–thick slices were obtained. Slices were placed in a Petri dish containing ACSF. Individual slices were then placed in an 8-well glass chamber (Lab-Tek) and 200 μL of ACSF was added to each well, with no liquid at the tissue-well interface to minimize interference with movie capture. A 0.5-μL PS bead suspension was added to the gray matter region. The 8-well chamber was then incubated at 37°C in humidity chamber for 30 minutes prior to imaging to allow tissue recovery and convection dissipation (44).

For rat brain tissue slices, all experiments were carried out at Johns Hopkins University School of Medicine in accordance with National Institutes of Health guidelines and local Institutional Animal Care and Use Committee regulations. Brain tissue slices were prepared from 130–160 g female Sprague-Dawley rats. Animals were anesthetized with ketamine-xylazine and then administered an intracardiac injection of Euthanosol. After euthanasia, the brain was rapidly removed and immersed in chilled ACSF supplemented with 10% glucose. Slices were processed and biodegradable particles were added in the same way as the human cortical slice preparation and PS particle addition above. MPT analysis is described in Supplementary methods.

Histopathological analysis of human brain slices

The human brain tissue slices were studied using standard hematoxylin and eosin (H&E) staining to identify any changes in histological architecture and cell morphology introduced by the preparation and incubation process. Representative tissue slices (n = 4) were preserved in formalin immediately following sectioning in the laboratory and after completing data acquisition, approximately 3 hours following removal, preparation, incubation, and particle imaging. The tissue was removed from the formalin after 24 hours and placed in 70% ethanol solution until paraffin embedding, sectioning, and H&E staining. The tissue sections were examined by a board-certified neuropathologist (C.E.) for evidence of tissue changes or damage.

In vivo mouse brain imaging

All experiments were approved by the Institutional Animal Care and Use Committee. The *in vivo* mouse model used was optimized to minimize tissue injury and brain movement with respect to imaging, and experiments were designed with knowledge of the potential contributions to particle movement by regional micro-pulsations from the dense network of surrounding blood vessels, as well as bulk flow phenomenon known to contribute to interstitial fluid circulation within the brain (45, 46). The cranial window technique was based on a modification from previously published studies (47, 48). To create a stable, immobile cranial window, a warm agarose solution (20% w/v) was placed over the exposed brain region and a 5-mm glass coverslip was quickly placed prior to agarose cooling and gelatinization. A custom circular metal bar was secured to the adjacent bone just lateral to the sagittal suture using a small drop of fast-drying adhesive. Cement (HyBond, Inc.) was then applied to secure the agarose, glass, and metal bar construct rigidly to the calvarium. A channel representing approximately 90 degrees of the cover glass circle was not cemented and left exposed for the glass pipette to insert into the brain.

The cranial bar was secured to a custom microscope stage allowing stable imaging of the anesthetized mouse. An upright confocal microscope (Zeiss, Inc.) with a two-photon laser source (Coherent Inc.) tuned to 910 nm was used for imaging through a 20× microscope objective [Zeiss Inc., Plan-Apochromat (NA, 1.0; working distance, 1.9 mm)]. Images were collected using a non-descanned detector. The micro-injection apparatus attached to a stereotactic manipulator (Drummond Scientific Inc.) was fixed with a glass micropipette (tip diameter ~30 μm), loaded with NP solution, and positioned for injection through the agarose channel into the brain. A blood vessel–free region of cortex was identified, and the micro-pipette was inserted to a depth of 100–200 μm below the pial surface under direct visualization, and withdrawn slightly to create a small pocket to receive the injection. The nano-injection device was set to inject 9.2 nL of particle solution at a rate of 23 nL/s. Particle combinations were mixed and injected at equivalent concentrations to each other and data was captured every 5 minutes for 60 minutes.

Statistical analysis

Statistical analysis of data was performed by one-way analysis of variance (ANOVA) follow by Tukey Honestly Significant Difference (HSD) or Games-Howell tests using SPSS 18.0 software (IBM Inc). Differences were considered statistically significant at $P<0.05$.

Supplementary Material

Refer to Web version on PubMed Central for supplementary material.

Acknowledgments

We thank F. Lenz, G. Jallo, A. Quinones-Hinojosa, W. Hsu, and J. Liauw for the help in providing human tissue samples. We thank H. Brem and B. Tyler for their advice and guidance on clinical applications and animal surgery techniques, respectively.

Funding: This work was supported by the National Institutes of Health, grants R01CA164789 and U54CA151838.

References and Notes

1. Wohlfart S, Gelperina S, Kreuter J. Transport of drugs across the blood-brain barrier by nanoparticles. Journal of controlled release : official journal of the Controlled Release. 2011
2. Serwer LP, James CD. Challenges in drug delivery to tumors of the central nervous system: an overview of pharmacological and surgical considerations. Adv Drug Deliv Rev. 2012; 64:590–597. [PubMed: 22306489]
3. Roney C, Kulkarni P, Arora V, et al. Targeted nanoparticles for drug delivery through the blood-brain barrier for Alzheimer's disease. Journal of controlled release : official journal of the Controlled Release Society. 2005; 108:193–214. [PubMed: 16246446]
4. Matsumura Y, Maeda H. A new concept for macromolecular therapeutics in cancer chemotherapy: mechanism of tumoritropic accumulation of proteins and the antitumor agent smancs. Cancer research. 1986; 46:6387–6392. [PubMed: 2946403]
5. Ambruosi A, Gelperina S, Khalansky A, et al. Influence of surfactants, polymer and doxorubicin loading on the anti-tumour effect of poly(butyl cyanoacrylate) nanoparticles in a rat glioma model. Journal of microencapsulation. 2006; 23:582–592. [PubMed: 16980278]
6. Kannan S, Dai H, Navath RS, et al. Dendrimer-based postnatal therapy for neuroinflammation and cerebral palsy in a rabbit model. Science translational medicine. 2012; 4 130ra146.
7. Reddy MK, Labhasetwar V. Nanoparticle-mediated delivery of superoxide dismutase to the brain: an effective strategy to reduce ischemia-reperfusion injury. FASEB J. 2009; 23:1384–1395. [PubMed: 19124559]

8. Brigger I, Morizet J, Aubert G, et al. Poly(ethylene glycol)-coated hexadecylcyanoacrylate nanospheres display a combined effect for brain tumor targeting. J Pharmacol Exp Ther. 2002; 303:928–936. [PubMed: 12438511]
9. Calvo P, Gouritin B, Chacun H, et al. Long-circulating PEGylated polycyanoacrylate nanoparticles as new drug carrier for brain delivery. Pharm Res. 2001; 18:1157–1166. [PubMed: 11587488]
10. Gref R, Minamitake Y, Peracchia MT, et al. Biodegradable long-circulating polymeric nanospheres. Science. 1994; 263:1600–1603. [PubMed: 8128245]
11. Patel T, Zhou J, Piepmeier JM, et al. Polymeric nanoparticles for drug delivery to the central nervous system. Adv Drug Deliv Rev. 2011
12. Degen JW, Walbridge S, Vortmeyer AO, et al. Safety and efficacy of convection-enhanced delivery of gemcitabine or carboplatin in a malignant glioma model in rats. J Neurosurg. 2003; 99:893–898. [PubMed: 14609170]
13. Bobo RH, Laske DW, Akbasak A, et al. Convection-enhanced delivery of macromolecules in the brain. Proc Natl Acad Sci U S A. 1994; 91:2076–2080. [PubMed: 8134351]
14. Allard E, Passirani C, Benoit JP. Convection-enhanced delivery of nanocarriers for the treatment of brain tumors. Biomaterials. 2009; 30:2302–2318. [PubMed: 19168213]
15. Pluen A, Boucher Y, Ramanujan S, et al. Role of tumor-host interactions in interstitial diffusion of macromolecules: cranial vs. subcutaneous tumors. Proc Natl Acad Sci U S A. 2001; 98:4628–4633. [PubMed: 11274375]
16. Thorne RG, Nicholson C. In vivo diffusion analysis with quantum dots and dextrans predicts the width of brain extracellular space. Proc Natl Acad Sci U S A. 2006; 103:5567–5572. [PubMed: 16567637]
17. Langer R. Drug delivery and targeting. Nature. 1998; 392:5–10. [PubMed: 9579855]
18. Lai SK, O'Hanlon DE, Harrold S, et al. Rapid transport of large polymeric nanoparticles in fresh undiluted human mucus. Proc Natl Acad Sci U S A. 2007; 104:1482–1487. [PubMed: 17244708]
19. Wang YY, Lai SK, Suk JS, et al. Addressing the PEG mucoadhesivity paradox to engineer nanoparticles that "slip" through the human mucus barrier. Angew Chem Int Ed Engl. 2008; 47:9726–9729. [PubMed: 18979480]
20. Amsden B. An obstruction-scaling model for diffusion in homogeneous hydrogels. Macromolecules. 1999; 32:874–879.
21. Lai SK, Wang YY, Hida K, et al. Nanoparticles reveal that human cervicovaginal mucus is riddled with pores larger than viruses. Proc Natl Acad Sci U S A. 2010; 107:598–603. [PubMed: 20018745]
22. Peters A. Golgi, Cajal, and the fine structure of the nervous system. Brain Res Rev. 2007; 55:256–263. [PubMed: 17270274]
23. van Harreveld A. Extracellular space in the central nervous system. Proc K Ned Akad Wet C. 1966; 69:17–21. [PubMed: 4222181]
24. Rice ME, Nicholson C. Diffusion characteristics and extracellular volume fraction during normoxia and hypoxia in slices of rat neostriatum. J Neurophysiol. 1991; 65:264–272. [PubMed: 2016641]
25. Ibata Y, Piccoli F, Pappas GD, et al. An electron microscopic and biochemical study on the effect of cyanide and low Na+ on rat brain slices. Brain Res. 1971; 30:137–158. [PubMed: 5092623]
26. de Bouard S, Christov C, Guillamo JS, et al. Invasion of human glioma biopsy specimens in cultures of rodent brain slices: a quantitative analysis. J Neurosurg. 2002; 97:169–176. [PubMed: 12134908]
27. Chaichana KL, Capilla-Gonzalez V, Gonzalez-Perez O, et al. Preservation of glial cytoarchitecture from ex vivo human tumor and non-tumor cerebral cortical explants: A human model to study neurological diseases. J Neurosci Methods. 2007; 164:261–270. [PubMed: 17580092]
28. Hajos F, Gerics B, Sotonyi P. Slices from the rat olfactory bulb maintained in vitro. Morphological aspects. J Neurosci Methods. 1992; 44:225–232. [PubMed: 1474854]
29. Larkman AU, Mason A, Blakemore C. The in vitro slice preparation for combined morphological and electrophysiological studies of rat visual cortex. Neurosci Res. 1988; 6:1–19. [PubMed: 3200517]

30. Tang BC, Dawson M, Lai SK, et al. Biodegradable polymer nanoparticles that rapidly penetrate the human mucus barrier. Proc Natl Acad Sci U S A. 2009; 106:19268–19273. [PubMed: 19901335]
31. Ensign LM, Tang BC, Wang YY, et al. Mucus-penetrating nanoparticles for vaginal drug delivery protect against herpes simplex virus. Science translational medicine. 2012; 4 138ra179.
32. Kim DH, Martin DC. Sustained release of dexamethasone from hydrophilic matrices using PLGA nanoparticles for neural drug delivery. Biomaterials. 2006; 27:3031–3037. [PubMed: 16443270]
33. Wong C, Stylianopoulos T, Cui J, et al. Multistage nanoparticle delivery system for deep penetration into tumor tissue. Proc Natl Acad Sci U S A. 2011; 108:2426–2431. [PubMed: 21245339]
34. Ambruosi A, Khalansky AS, Yamamoto H, et al. Biodistribution of polysorbate 80-coated doxorubicin-loaded [14C]-poly(butyl cyanoacrylate) nanoparticles after intravenous administration to glioblastoma-bearing rats. Journal of drug targeting. 2006; 14:97–105. [PubMed: 16608736]
35. Kulkarni SA, Feng SS. Effects of surface modification on delivery efficiency of biodegradable nanoparticles across the blood-brain barrier. Nanomedicine (Lond). 2011; 6:377–394. [PubMed: 21385139]
36. Na JH, Koo H, Lee S, et al. Real-time and non-invasive optical imaging of tumor-targeting glycol chitosan nanoparticles in various tumor models. Biomaterials. 2011; 32:5252–5261. [PubMed: 21513975]
37. Cragg B. Preservation of extracellular space during fixation of the brain for electron microscopy. Tissue Cell. 1980; 12:63–72. [PubMed: 6987773]
38. Sykova E, Nicholson C. Diffusion in brain extracellular space. Physiol Rev. 2008; 88:1277–1340. [PubMed: 18923183]
39. Vyas V, Podesta A, Milani P. Probing nanoscale interactions on biocompatible cluster-assembled titanium oxide surfaces by atomic force microscopy. J Nanosci Nanotechnol. 2011; 11:4739–4748. [PubMed: 21770100]
40. Pamujula S, Hazari S, Bolden G, et al. Cellular delivery of PEGylated PLGA nanoparticles. The Journal of pharmacy and pharmacology. 2012; 64:61–67. [PubMed: 22150673]
41. Mert O, Lai SK, Ensign L, et al. A poly(ethylene glycol)-based surfactant for formulation of drug-loaded mucus penetrating particles. Journal of controlled release : official journal of the Controlled Release Society. 2012; 157:455–460. [PubMed: 21911015]
42. McDannold N, Arvanitis CD, Vykhodtseva N, et al. Temporary disruption of the blood-brain barrier by use of ultrasound and microbubbles: safety and efficacy evaluation in rhesus macaques. Cancer research. 2012
43. Popielarski SR. A nanoparticle-based model delivery system to guide the rational design of gene delivery to the liver. 1. Synthesis and characterization. Bioconjug Chem. 2005; 16
44. Rambani K, Vukasinovic J, Glezer A, et al. Culturing thick brain slices: an interstitial 3D microperfusion system for enhanced viability. J Neurosci Methods. 2009; 180:243–254. [PubMed: 19443039]
45. Abbott NJ. Evidence for bulk flow of brain interstitial fluid: significance for physiology and pathology. Neurochem Int. 2004; 45:545–552. [PubMed: 15186921]
46. Sato O, Bering EA Jr, Yagi M, et al. Bulk flow in the cerebrospinal fluid system of the dog. Acta Neurol Scand. 1975; 51:1–11. [PubMed: 1119314]
47. Bock DD, Lee WC, Kerlin AM, et al. Network anatomy and in vivo physiology of visual cortical neurons. Nature. 2011; 471:177–182. [PubMed: 21390124]
48. Holtmaat A, Bonhoeffer T, Chow DK, et al. Long-term, high-resolution imaging in the mouse neocortex through a chronic cranial window. Nat Protoc. 2009; 4:1128–1144. [PubMed: 19617885]
49. Rizzo V, Pinciroli V. Quantitative NMR in synthetic and combinatorial chemistry. Journal of pharmaceutical and biomedical analysis. 2005; 38:851–857. [PubMed: 16087047]
50. Yoo HS, Oh JE, Lee KH, et al. Biodegradable nanoparticles containing doxorubicin-PLGA conjugate for sustained release. Pharm Res. 1999; 16:1114–1118. [PubMed: 10450940]
51. Valentine MT, Perlman ZE, Gardel ML, et al. Colloid surface chemistry critically affects multiple particle tracking measurements of biomaterials. Biophys J. 2004; 86:4004–4014. [PubMed: 15189896]

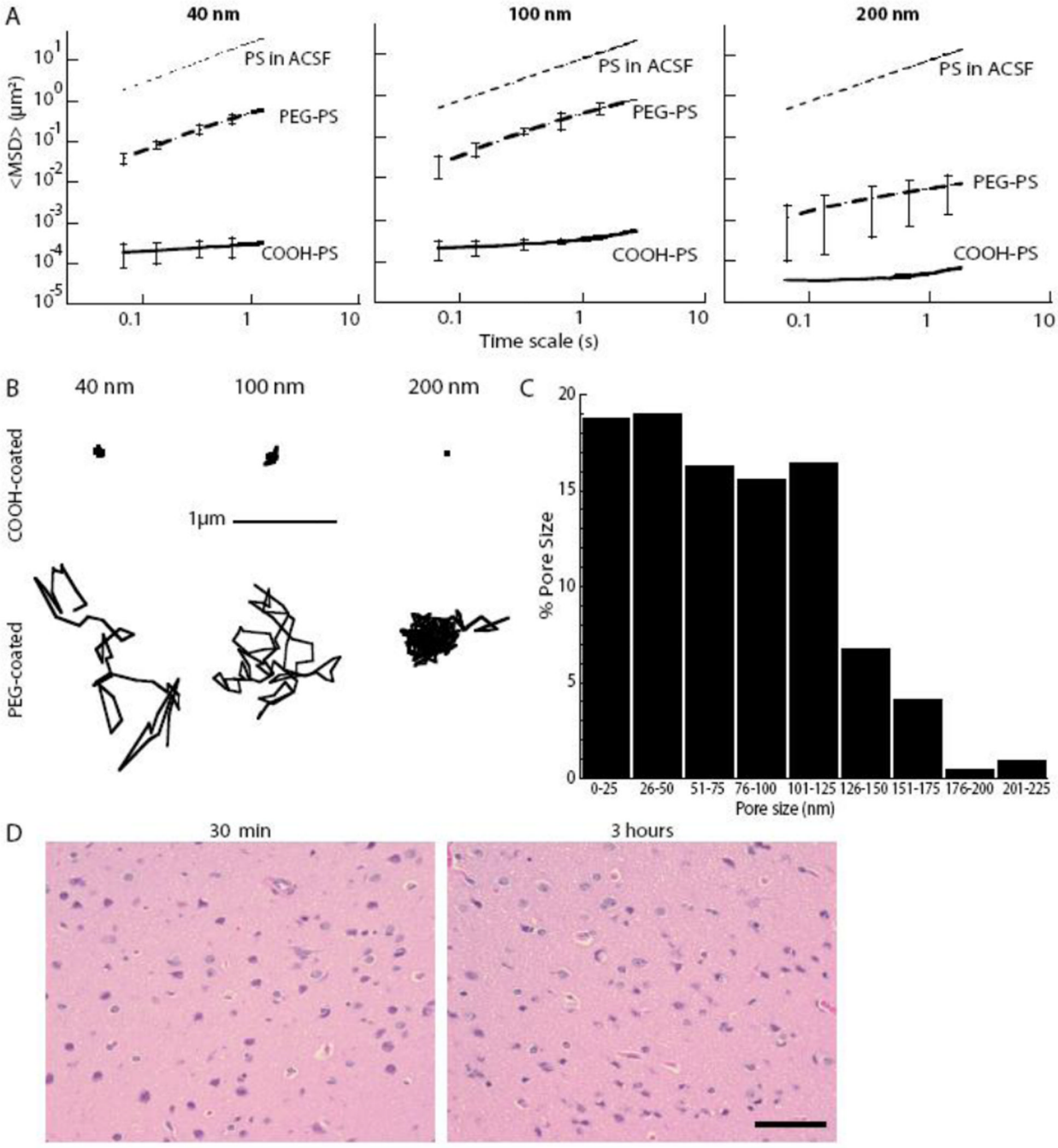

Figure 1. Nanoparticle penetration of human brain tissue *ex vivo*

(**A**) Ensemble-averaged geometric mean square displacements (<MSD>) as a function of time scale for 40 nm, 100 nm, and 200 nm PEG- and COOH-coated PS nanoparticles. Data represent the ensemble average of at least four independent experiments, with $n \geq 100$ particles for each experiment. For each experiment, the transport rates of all three particle sizes, with and without PEG coatings, were measured in the same brain tissue. Grey dotted lines indicate theoretical diffusivity values based on Stokes Einstein equation for the same size particles in ACSF. (**B**) Representative particle trajectories for COOH- and PEG-coated NPs of various sizes in human brain tissue. Trajectories shown are of particles that

possessed a <MSD> equal to the ensemble average at a time scale of 1 s. (**C**) The percent of pores that fall in a dedicated size range in the ECS of fresh human brain tissue. Pore size distribution approximation was based on diffusion rates of PEG-coated 100-nm NPs combined with an obstruction scaling model (14). Data represent the ensemble average of four independent experiments with $n > 100$ particles tracked for each experiment. (**D**) H&E-stained human cortical brain slices 30 min after removal and following MPT for 3 hours *ex vivo* in culture at 37°C. Scale bar, 40 μm.

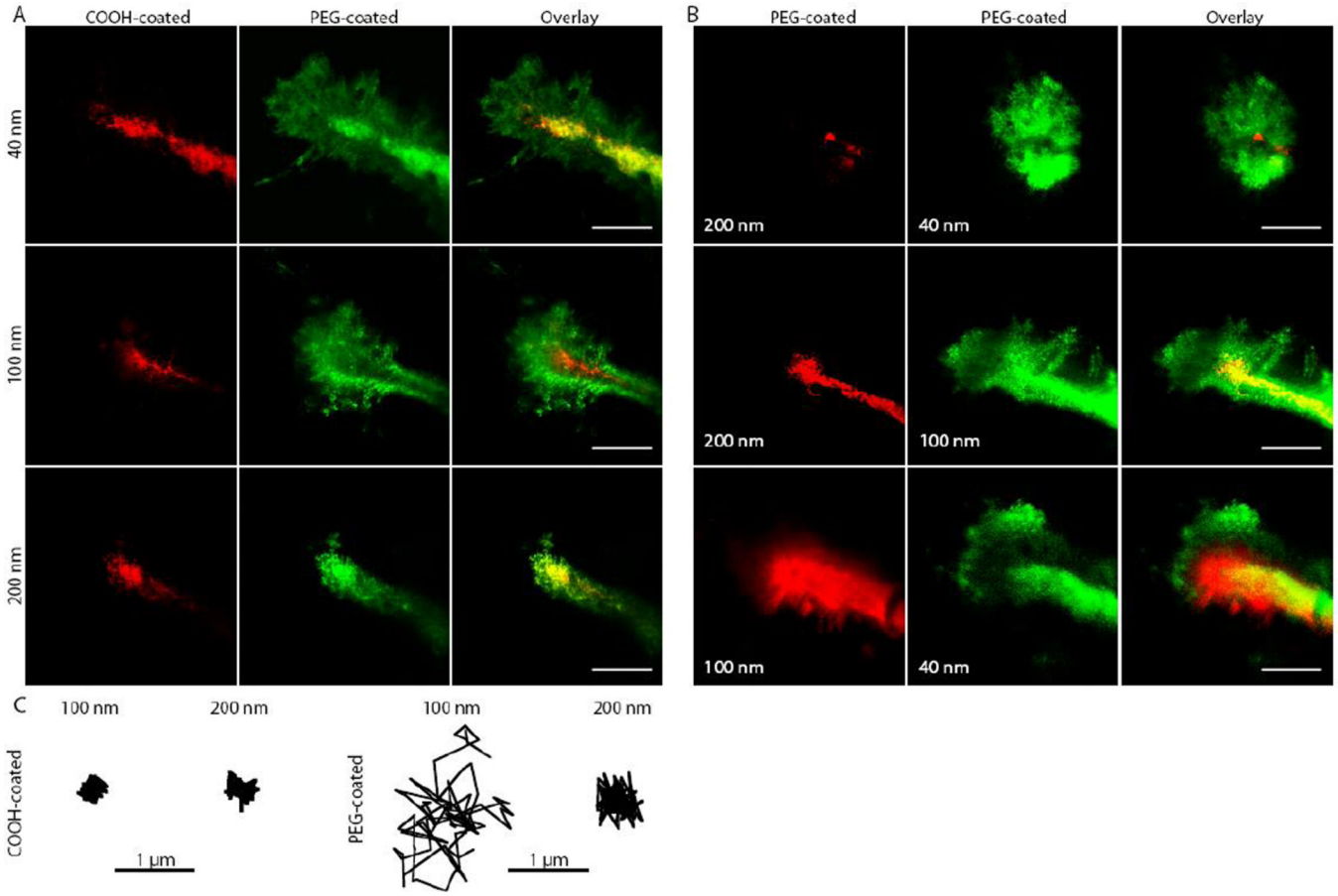

Figure 2. Nanoparticle penetration of brain tissue *in vivo* in living mice

Actual sizes of each particle type are listed in Table 1. (**A**) Direct comparison of the distribution of fluorescent NPs of similar sizes with different surface coatings following intracranial co-injection into mice. Images were acquired 60 min after injection. Scale bars, 50 μm. (**B**) Direct comparison of the distribution of PEG-coated NPs of various sizes following intracranial co-injection into mice. Images were acquired 60 min after injection. Scale bars, 50 μm. (**C**) Representative particle trajectories for COOH- and PEG-coated NPs in live mouse brain. Trajectories shown are of particles that possessed an <MSD> equal to the ensemble average at a time scale of 1 s, as determined by at least three independent experiments, with $n \geq 100$ particles tracked for each experiment.

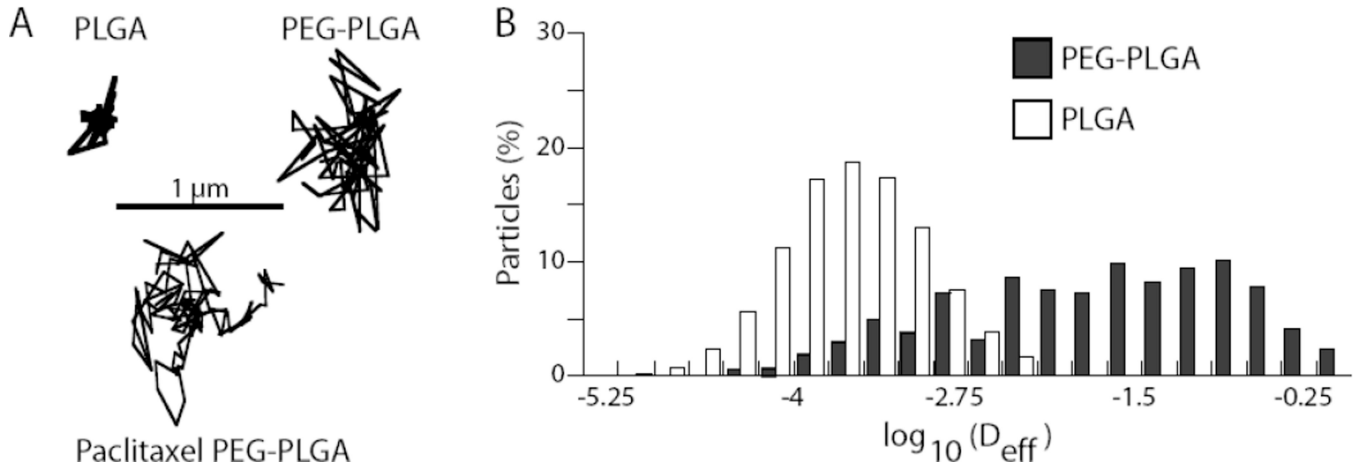

Figure 3. Transport of paclitaxel-loaded PEG-PLGA nanoparticles through rat brain tissue *ex vivo*

(**A**) Sample trajectories of PLGA, PEG-PLGA, and paclitaxel-loaded PEG-PLGA NPs in brain tissue. Trajectories reflect particles with effective diffusivities within one SEM of the ensemble average. (**B**) Distributions of the logarithms of individual particle effective diffusivities (D_{eff}) for PLGA and PEG-PLGA nanoparticles at a time scale of 1 s. Data represent means of at least three experiments, with $n \geq 100$ particles per experiment.

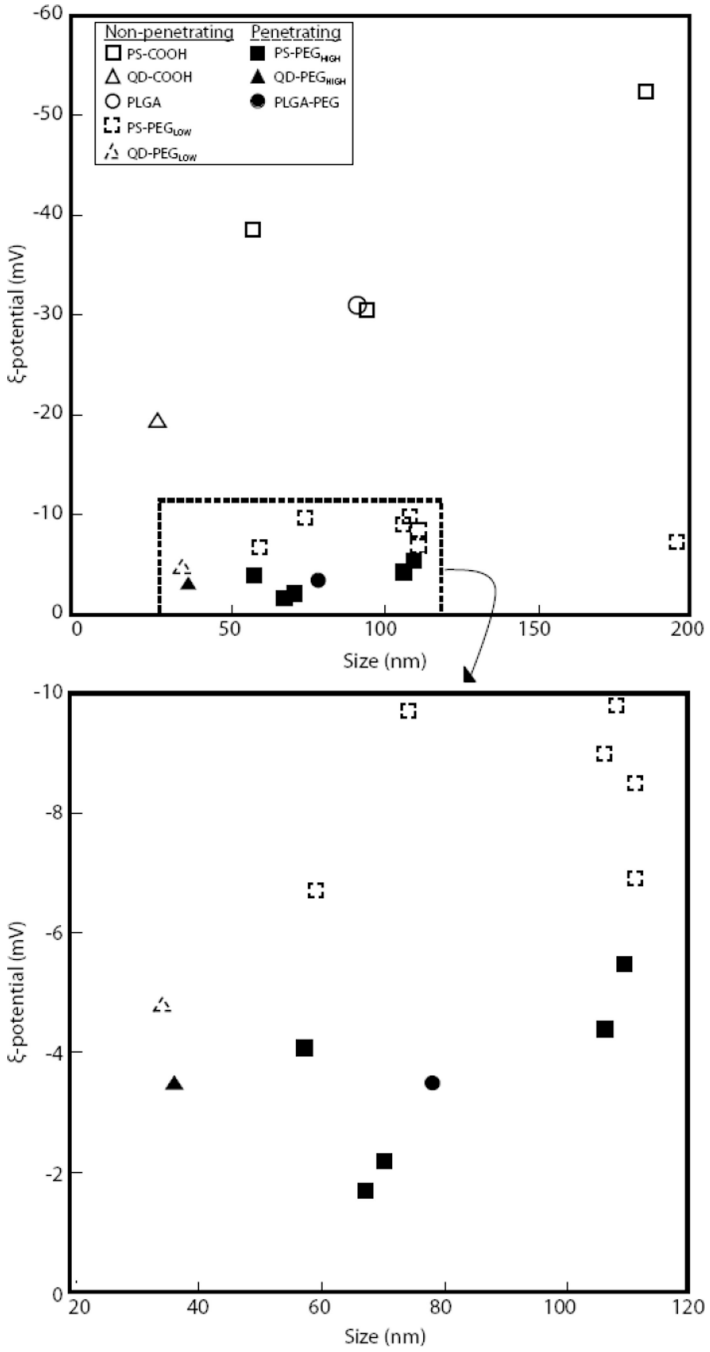

Figure 4. Phase diagram correlating ζ-potential and size to transport behavior

Data were obtained from rodent brain tissue *ex vivo* for various uncoated and PEG-coated nanoparticles ($n = 3$). Black-filled symbols indicate diffusive brain penetrating particles and open symbols indicate particles that are immobilized. The lower box is an expanded view of the indicated region in dotted box. Each data point represents one nanoparticle formulation.

Table 1

Physicochemical properties and diffusivity of polystyrene nanoparticles in normal human cortical tissue and in ACSF

Effective diffusivity of nanoparticles in normal brain tissue (D_b) was calculated at a time scale of 1 s. Nanoparticle diffusivity in ACSF (D_{ACSF}) was calculated using Stokes-Einstein equation and mean particle diameter. Size was provided by the manufacturer and actual diameter in ACSF at pH 7.0 was measured using dynamic light scattering. ζ-potential and PDI were measured in ACSF at pH 7.0. Size, ζ-potential, and PDI were all measured following 24 hour incubation in ACSF.

Size (nm)	Surface modification of PS nanoparticles	Mean diameter ± SEM (nm)	Mean ζ-potential ± SEM (mV)	PDI	D_{ACSF}/D_b
40	PEG	69 ± 2	−2.8 ± 0.4	0.05	37*
40	COOH	57 ± 2	−38.6 ± 2.5	0.04	85,000
100	PEG	106 ± 4	−4.4 ± 0.2	0.03	36*
100	COOH	94 ± 3	−30.5 ± 4.5	0.03	54,000
200	PEG	198 ± 6	−7.8 ± 0.6	0.03	1600*
200	COOH	185 ± 1	−52.4 ± 2.6	0.01	86,000

* $P < 0.05$ compared to COOH-PS (ANOVA).

Sci Transl Med. Author manuscript; available in PMC 2013 August 29.

Table 2

Effect of PEG coating density on nanoparticle penetration in rat brain tissue *ex vivo*

PEG surface density was calculated by NMR. Qualitative assessments of polystyrene NP movement, scaled as (−−−) representing immobile NPs and (+++) representing highly diffusive NPs, were obtained by real-time multiple particle tracking (MPT) of NPs in rat brain tissue *ex vivo* (n = 4 videos per each of 3 brain samples).

Mean particle diameter ± SEM (nm)	Mean ζ-potential ± SEM (mV)	PDI	PEG density (chains/100 nm^2)	Γ/SA	Qualitative MPT
119 ± 4	−9.8 ± 1.1	0.05	3	0.6	−−−
106 ± 3	−9.0 ± 0.8	0.03	3	0.7	−−−
111 ± 6	−8.5 ± 0.1	0.03	6	1.2	−−−
111 ± 3	−6.9 ± 0.5	0.04	7	1.7	−−
119 ± 1	−5.5 ± 0.4	0.02	9	2.1	++
106 ± 4	−4.4 ± 0.2	0.03	9	2.0	+++
114 ± 3	−2.5 ± 0.1	0.03	9	2.0	+++